

See discussions, stats, and author profiles for this publication at: <http://www.researchgate.net/publication/224098343>

Modeling of the laser pyrolysis process by means of the aerosol theory: Case of iron nanoparticles

ARTICLE in JOURNAL OF APPLIED PHYSICS · FEBRUARY 2010

Impact Factor: 2.18 · DOI: 10.1063/1.3273483 · Source: IEEE Xplore

CITATIONS

3

READS

24

5 AUTHORS, INCLUDING:



[Oscar Bomati-Miguel](#)

Universidad Autónoma de Madrid

56 PUBLICATIONS 867 CITATIONS

SEE PROFILE



[Xinqing Zhao](#)

Beihang University(BUAA)

63 PUBLICATIONS 709 CITATIONS

SEE PROFILE



[Stefano Martelli](#)

Centro Sviluppo Materiali S.p.A.

92 PUBLICATIONS 811 CITATIONS

SEE PROFILE



[Paolo Emilio Di Nunzio](#)

Centro Sviluppo Materiali S.p.A.

29 PUBLICATIONS 178 CITATIONS

SEE PROFILE

Modeling of the laser pyrolysis process by means of the aerosol theory: Case of iron nanoparticles

O. Bomati-Miguel,¹ X. Q. Zhao,² S. Martelli,³ P. E. Di Nunzio,³ and S. Veintemillas-Verdaguer^{4,a)}

¹Networking Research Centre on Bioengineering, Biomaterials and Nanomedicine (CIBER-BBN), Nanoporous Films and Particles (NFP), INA, Zaragoza, Spain

²School of Materials Science and Engineering, Beijing University of Aeronautics and Astronautics, Beijing 100083, People's Republic of China

³Centro Sviluppo Materiali, Via di Castel Romano 100, 00128 Rome, Italy

⁴Institute of Materials Science of Madrid (CSIC), Cantoblanco, 28049 Madrid, Spain

(Received 20 August 2009; accepted 13 November 2009; published online 5 January 2010)

Laser pyrolysis is a technique in which the interaction between a laser and a gaseous flow of precursors is used to obtain homogeneous nanoparticles. One of the main advantages of using this method is that it generates ultrafine powders in a continuous way with narrow particle-size distribution. The absence of surfactants of potential toxicity makes the product ideal for the preparation of colloidal dispersions for use in biomedical applications. It is of particular interest in the case of the iron nanoparticles due to their high magnetic response. In this paper, a simple coagulation model adapted from the theory of aerosol formation is successfully used in the modeling of the production of iron nanoparticles. The experimental conditions needed to maximize the productivity were obtained as a function of particle size. The main conclusion is that for the production of “large” particle-size nanomaterials (>20 nm), the ruling factors are the pressure and the carrier gas flux. However, the production of small particle-size nanomaterials (<20 nm) depends on the evaporation temperature of the precursor. © 2010 American Institute of Physics. [doi:10.1063/1.3273483]

I. INTRODUCTION

Fashionable magnetic nanoproboscopes have revolutionized the face of *in vivo* molecular imaging, diagnosis, and tumor-treatment techniques.^{1–3} Nowadays, most of the magnetic probes used for *in vivo* detection, imaging, and local treatment of malignant tumor cells are based on magnetic nanoparticles.^{4–6} However, to transfer these nanoproboscopes from the laboratory to the clinical environment is a severe problem. This is due to the difficulties that arise in the existing industrial-scale synthesis methods used to produce homogeneous samples of pure magnetic nanoparticles with precise control of particle shape and size distribution. All the mentioned characteristics influence the magnetic and colloidal properties of the aqueous dispersions made with the powders, which are critical issues for their application in biomedicine. Therefore, recently many attempts have been made to develop new preparative methods to achieve all the above-mentioned goals.

Currently, the synthesis of magnetic nanoparticles is carried out by a large variety of chemical and physical manufacturing processes.^{7–9} Among the different synthetic routes, laser-induced pyrolysis could fulfill all the above-mentioned requirements. This method was first reported by Haggerty and Cannon^{10–12} for use in the preparation of ceramic powders, such as Si, Si₃N₄, and SiC, by means of thermal decomposition reactions of different gas-phase organometallic precursors exposed to the laser radiation. The photons be-

have as highly selective reactants that energize certain chemical species selectively, depending on their wavelength. The energy is then transmitted to the rest of the reactant gas mixtures in a short time, and the nanoparticles are generated. This technique enables us to explore new synthesis strategies for nanoparticles that are not available when using traditional synthesis routes based on chemical reactions in solution or on standard chemical vapor deposition procedures in a furnace.

In particular, the laser pyrolysis of iron pentacarbonyl vapors has been recently reported to produce core-shell Fe@Fe₂O₃ magnetic nanoparticles with sizes ranging from 10 to 30 nm narrow particle-size distribution and high-saturation magnetization by strong infrared irradiation of the precursor by a high power CO₂ laser.¹³ These particles were used with good results to prepare pharmaceutical-grade magnetic colloidal dispersions to be used as *in vivo* magnetic resonance imaging contrast enhancement agents.¹⁴ In the same way, Swihart *et al.*¹⁵ reported the production of strongly red-luminescent, monodispersed silicon nanoparticles with sizes smaller than 10 nm by decomposition of silane gas. The viability of these nanoparticles as fluorescence imaging optical-contrast enhancement agents was tested with good results.¹⁶

Despite the obvious advantages that the laser-induced pyrolysis technique provides for the synthesis of magnetic and nonmagnetic nanoparticles, only a few attempts have been made to understand the physical basis for the formation of nanometric particles in this technique and to understand the effect of the process variables on particle size, the most

^{a)}Electronic mail: sabino@icmm.csic.es.

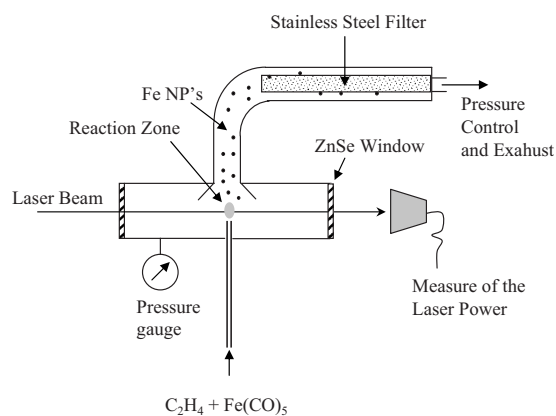


FIG. 1. Schematic representation of the laser pyrolysis apparatus used in the synthesis of ultrafine powders.

important attempt being the use of the classical nucleation theory reported by Lihrmann and Cauchetier.¹⁷ Recently, we (P.E.D.N. and S.M.) reported a mathematical model that explained the aggregation and coagulation process that takes place during the growth of silicon nanoparticles synthesized by laser-induced pyrolysis.¹⁸ By using the same physical model, in this current work the effect of the process conditions on the size of iron nanoparticles produced by laser pyrolysis was analyzed. Finally, the optimum experimental conditions for the production of iron nanoparticles of a given size were determined.

II. EXPERIMENTAL

A. Particle production

The method of synthesis of nanoparticles by laser pyrolysis consists of the heating of a flowing mixture of gases using a continuous wave carbon dioxide laser, which both initiates and sustains the chemical reaction. A small reaction zone is defined by the overlap between the vertical reactant gas stream and the horizontal laser beam. The reaction zone is placed safely away from the chamber walls. This design provides an ideal environment for the nucleation of small particles in the nanometer range, with less contamination and a narrower size distribution than those prepared by more conventional thermal methods.¹⁹ Reagent-grade iron pentacarbonyl, obtained from Aldrich Chemical Inc., was used as an iron precursor due to its high-vapor pressure and easy decomposition. It was stored in the dark at 7 °C under nitrogen and was employed without purifying. Due to the absence of absorption bands of this compound at the laser wavelength ($10.60 \pm 0.05 \mu\text{m}$), ethylene was used as an absorbent gas as well as a carrier gas. Ethylene simply absorbs the laser radiation; it heats the gas mixture and induces the decomposition of iron pentacarbonyl into iron and carbon monoxide, but does not decompose itself under the laser densities of energy used in the experiments. Above a certain pressure and laser intensity, a critical concentration of product nuclei is formed in the reaction zone, leading to the homogeneous nucleation and growth of iron particles collected on a filter. A schematic representation of the experimental CO₂ laser pyrolysis setup used in this work is shown in Fig. 1. The range of experimental conditions in which pure iron

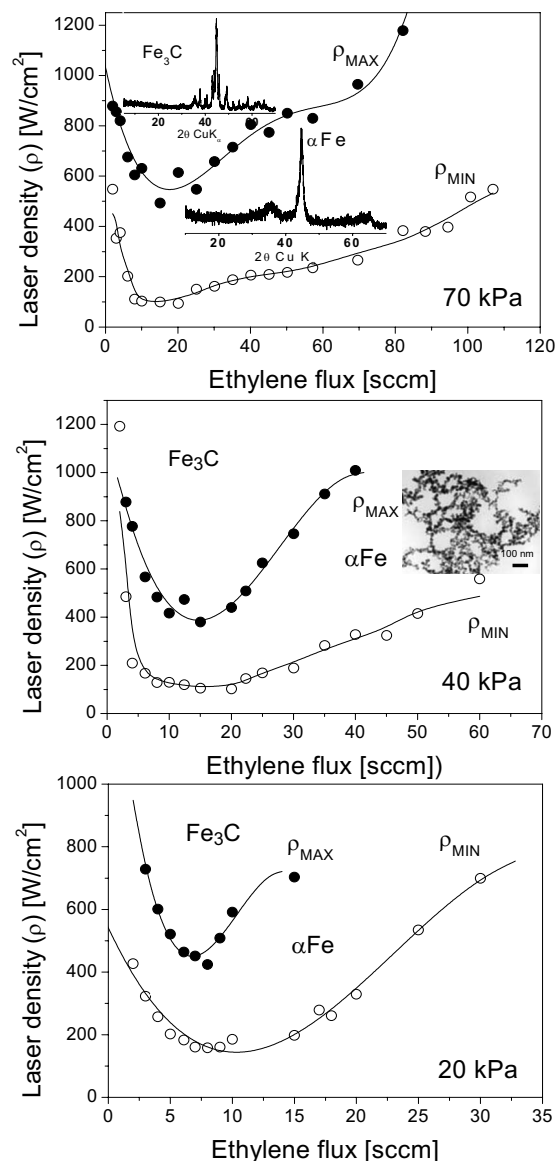


FIG. 2. Experimental conditions available for the synthesis of α -Fe nanocrystals by laser pyrolysis in the system $\text{Fe}(\text{CO})_5$ (vapor)– C_2H_4 . The possible experimental conditions are located between the upper and lower laser density curves. The insets show the powder diffraction patterns of the samples obtained and the general appearance of an α -Fe sample under the transmission electron microscope.

nanoparticles are produced is depicted in Fig. 2. Below the low laser density curves, no pyrolysis arises, and above the upper laser density curves, iron carbides are formed.²⁰

B. Measurement of the process temperature

Measuring temperature is difficult in the laser pyrolysis process because the presence of the laser precludes the introduction of any device in the reaction zone. Only optical systems can be used, but their effectiveness is restricted to strong light-emission processes obtained at high laser intensities.^{10–12} As mentioned, to avoid the production of the undesired iron carbide, high laser intensities could not be used in our case. The process takes place under low-emission conditions, which make the standard infrared pyrometers useless. This problem was solved by measuring the tempera-

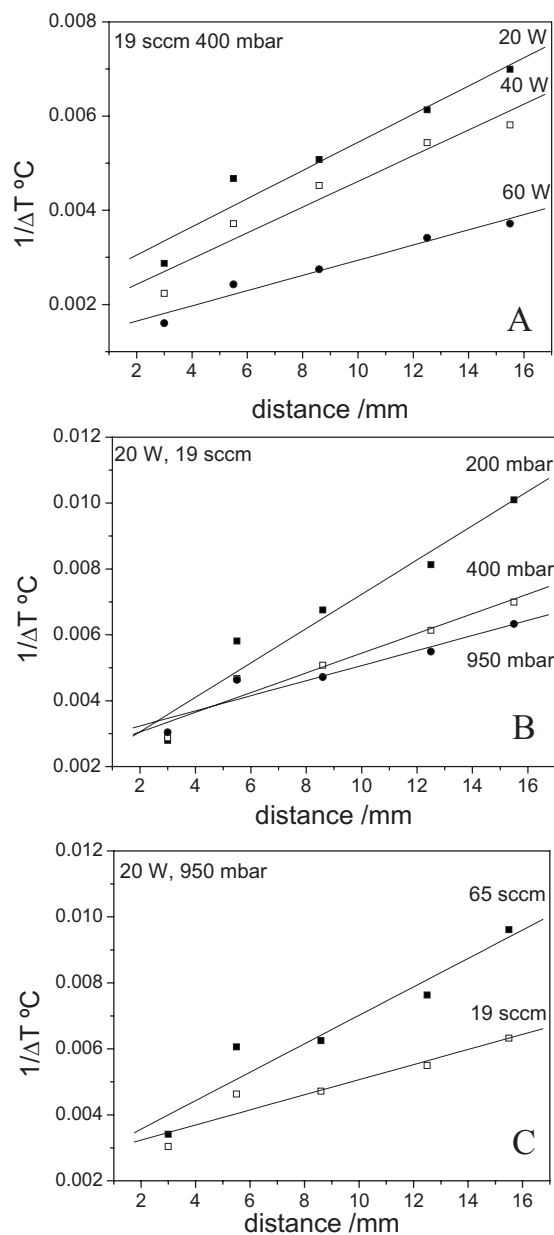


FIG. 3. Several plots of the inverse of the increment of temperature present in the gas flow as a function of the distance from the exit of the laser beam. The maximum temperature increment attained by the gas is obtained from the ordinate values of the adjusted lines at the origin.

ture profile in the gas mixture along the reaction plume immediately after irradiation by means of a series of five equidistant K-type thermocouples. From the linear plot of the reciprocal temperature $1/T$ versus the distance from the nozzle, the maximum temperature increase ΔT_{\max} was obtained as the intercept at the origin. Due to the fast clogging of the thermocouples by the iron powders, the temperature measurements were carried out with pure ethylene only, assuming that the low concentration of iron precursor (around 1%) does not influence the temperature very much. In Fig. 3, several plots of $1/T$ versus distance are presented for different experimental conditions. From Fig. 3(a), where the effect of the laser power is presented, one can see that as expected, the increase in laser power raises the reaction temperature (and decreases the origin intercept), whereas the total pres-

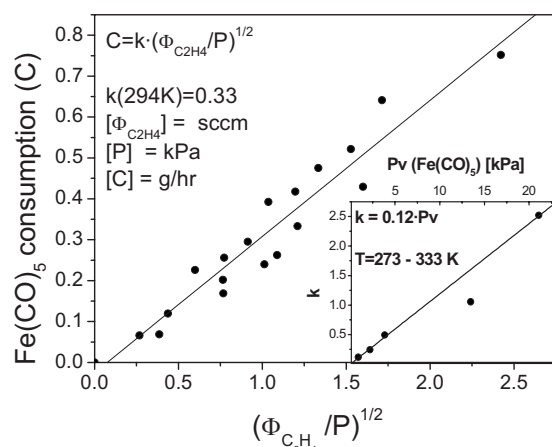


FIG. 4. An adjustment of a single constant empirical expression for the consumption rate of iron pentacarbonyl as a function of the ethylene flux and the pressure. In the inset is depicted the dependence of the empirical constant to the vapor pressure of the iron precursor.

sure and the ethylene flux have less effect on it [Figs. 3(b) and 3(c)]. Using linear multivariable standard procedures, the following empirical equations for ΔT_{\max} were obtained:

$$\Delta T_{\max} = 206 + 5.8W(W) - \frac{1500}{\Phi(\text{sccm})} + \frac{8600}{P(\text{kPa})} \quad (1)$$

($r=0.97$, 12 points, 6% error, 20–60 W, 19–65 sccm, 20–95 kPa).

C. Measurement of the consumption rates

One of the main inputs of the calculations is the input of the iron precursor. In a series of experiments, the average consumption rate of iron pentacarbonyl was measured by weighing the precursor bottle before and after the process as a function of the reaction temperature, the ethylene flux, and the chamber pressure.

It has been found that at room temperature, a linear relation exists between the consumption rate and the square root of the ratio between the ethylene flux and the pressure, as shown in Fig. 4. Since the slope of this expression scales linearly with the vapor pressure of carbonyl²¹ (see inset of Fig. 4), the following expressions for the evaluation of the consumption rate can be used:

$$C(\text{g/h}) = 0.12Pv(\text{kPa}) \sqrt{\frac{\Phi(\text{sccm})}{P(\text{kPa})}},$$

$$Pv(\text{kPa}) = 0.133 \times 10^{8.496 - 2097/T(\text{K})},$$

$$\Phi_{\text{Fe(CO)}_5}(\text{sccm}) = C(\text{g/h}) \times 1.905 \quad (2)$$

($r=0.96$, 19 points, 5% error, 19–65 sccm, 20–95 kPa, 273–333 K).

III. PHYSICO-CHEMICAL MODEL OF IRON NANOPARTICLE FORMATION

A. Fundamental principles of aerosol theory

Using the classical nucleation theory, the critical radius estimated for iron nuclei at the very high supersaturation

levels attained in this system is always similar to—or even smaller than—the atomic iron radius. This allows us to ignore the nucleation stage and describe the condensation process of the nanoparticles as a coagulation process where pairs of particles just collide to form bigger ones.

The analytical description of the coagulation kinetics of particles can be approached by analogy with the theory of aerosols.²² Then, coagulation is supposed to occur by collisions between pairs of particles, and each impact is assumed to be effective. In the absence of force fields acting on particles, two limiting hypotheses can be made on the mechanism responsible for collision coagulation, depending on the mean free path of molecules in the gas and on the particle size. If the mean free path in the gas (λ) is much larger than the average particle size (d), then a free-molecule regime can be assumed for the system. Otherwise a viscous diffusion regime (continuum regime) controls the coarsening kinetics. The Knudsen number (Kn) is defined as

$$\text{Kn} = \frac{2\lambda}{d}. \quad (3)$$

A pure free-molecule regime exists for Kn greater than 50, whereas a pure continuum regime can be considered for Kn below 4.²² Other authors define the free-molecule regime for Knudsen numbers above 20.²³ In the present case $\lambda = 10^{-3} - 6 \times 10^{-3}$ cm [using for the molecular diameter of iron the value of 2.52×10^{-8} cm (Ref. 21) and $d < 4 \times 10^{-6}$ cm]; therefore the minimum value of Kn is about 500 and the nanoparticle formation occurs in the free-molecule regime.

Collisions are the elementary steps of the bimolecular coagulation reaction. After each effective collision, the number of particles decreases by 1 unit. The kinetic equation can be written as

$$\frac{dN}{dt} = -\beta, \quad (4)$$

where N is the number of particles per unit of volume in a given time (t) and β is the number of collisions per unit of volume and time. In the present formalism, the system of colliding particles is treated as monodispersed, even if it is apparently not the case. If particles are small enough to move in a free-molecule regime during the whole process, the kinetic theory of gases can be used to estimate the collision rate as follows:^{22,24}

$$\beta = \frac{1}{\sqrt{2}} (\pi d^2) \left(\frac{8kT}{\pi m} \right)^{1/2} N^2, \quad (5)$$

where πd^2 is the geometrical collision cross section, k is the Boltzmann constant, T is the absolute temperature, and m is the mass of the particle. The last term is the average particle velocity in the gas. At a first approximation, this can be regarded as a second order kinetics, being $\beta \propto N^2$. To solve more rigorously Eq. (5), it is necessary to express in terms of N the quantities d and m . This can be done by taking into account the mass balance expressed as

$$\varphi = NV = N_0 V_0, \quad (6)$$

where φ is the volume fraction of the coarsening phase in the system (constant through the whole process), N_0 is the initial number of atoms in the gas per unit volume, V_0 is their volume, and V is the current average particle volume in a given time. Therefore, for spherical particles, the average diameter is

$$d = \left(\frac{6V}{\pi} \right)^{1/3} = \left(\frac{6N_0 V_0}{\pi N} \right)^{1/3}. \quad (7)$$

Similarly, the average particle mass is

$$m = \rho V = \rho \frac{N_0 V_0}{N}, \quad (8)$$

where ρ is the iron density (7.86 g/cm³) and V_0 is the atomic volume of iron (8.379×10^{-24} cm³).²¹ Substituting Eqs. (8), (9), and (6) into Eq. (5) and rearranging, one obtains

$$\frac{dN}{dt} = -KN^{11/6}, \quad (9)$$

$$K = 6^{2/3} \left(\frac{4kT}{\rho} \right)^{1/2} \left(\frac{N_0 V_0}{\pi} \right)^{1/6}.$$

It can be observed that the kinetic equation is not modified substantially by the insertion of the functional dependency of the particle size and mass on the particle density (N) because the order of reaction is close to 2. By integrating with the initial condition $N(t=0) = N_0$, the following result is obtained:

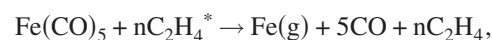
$$N(t) = \left[N_0^{-5/6} + \frac{5}{6} Kt \right]^{-6/5}. \quad (10)$$

Accordingly, from Eq. (7), the evolution of the average particle size with time is given by

$$d(t) = \left(\frac{6N_0 V_0}{\pi} \right)^{1/3} \left[N_0^{-5/6} + \frac{5}{6} Kt \right]^{2/5}. \quad (11)$$

B. Application to the coagulation of iron nanoparticles produced by laser pyrolysis

Different authors have demonstrated that the formation of iron nanoparticles by laser-induced decomposition of iron pentacarbonyl takes place according to the following scheme:^{25,26}



According to this, the infrared radiation is absorbed by the nonreacting molecule of C₂H₄ present in the gas mixture, which attains a vibrationally excited state denoted by an asterisk. This energy is transmitted through collisions to iron pentacarbonyl molecules, which dissociate into gaseous iron

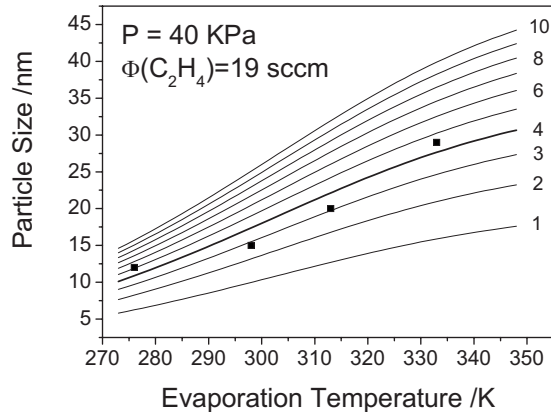


FIG. 5. Plot of the particle sizes obtained as a function of the evaporation temperature. Other experimental conditions remained constant for several coagulation times (t_c) in milliseconds. The solid points represent the experimental data.

atoms and carbon monoxide, returning C_2H_4 to the fundamental state. Finally, the gaseous iron atoms coagulate to form ultrafine particles.

A complete dissociation of the gaseous precursor is assumed when the gas temperature reaches the experimentally determined dissociation temperature of 523 K.²⁷ The number of iron nanoparticles generated in a volume unit of the gas stream at this temperature is calculated from the control parameters of the system as follows:

$$N_0 = \frac{\Phi_{\text{carbonyl}}}{\Phi_{\text{ethylene}} + 6\Phi_{\text{carbonyl}}} \frac{P}{kT}, \quad (13)$$

where it is considered that the decomposition of one molecule of precursor produces six molecules of gaseous products, P is the total pressure, and T is the average coagulation temperature.

In order to apply Eq. (11) to calculate the final particle size, it is necessary to know the coagulation temperature and

the reaction time. These parameters are difficult to estimate, and they constitute the main problem in the application of the theory. In this work, we assume that the process takes place at the temperature reached at the exit of the laser beam $298 + \Delta T_{\text{max}}$. This is supported by the repeated observation of visible flames, where the most brilliant zone coincides with the laser-exit zone. As mentioned in Sec. II, this temperature could be obtained by extrapolation from the thermal profiles measured in the reaction plume [Eq. (1)]. The estimation of the coagulation time (t_c) is more difficult due to the uncertainty in the start and finish time of the process. In this work, the coagulation time is considered as an adjustable parameter.

1. Determination of the coagulation time

For a set of experiments in which only the evaporation temperature is modified, it is reasonable to assume that the coagulation time should be roughly the same. In Fig. 5, the particle diameters predicted by the theory are plotted for different coagulation times in the range from 1 to 10 ms as a function of the evaporation temperature. By overlapping this graph with the experimental sizes determined by transmission electron microscopy (TEM), it is clearly seen that all of them are close to the line corresponding to 4 ms for the experimental conditions of the experiments. This indicates that the assumption of nondependence of coagulation time on evaporation temperature was correct and gives an approximate value for it.

In order to use the theory to calculate particle size as a function of the process parameters (laser intensity, ethylene flux, pressure, and evaporation temperature), an estimation of the coagulation time was carried out for a set of 14 laser pyrolysis experiments using the same plot presented in Fig. 5. The results are shown in Table I. Using a linear multivariate analysis, the following expression for the reaction time as a function of the process parameters was obtained:

TABLE I. Effect of the process conditions on the particle size of the iron nanoparticles obtained by laser pyrolysis (evaporation temperature of 25 °C).

| Experimental data | | | | Coagulation time (ms) | | Calculated |
|---------------------|----------------------|----------------|---------------------------------------|-----------------------|-------------------|--------------------|
| Laser intensity (W) | Ethylene flux (sccm) | Pressure (kPa) | Particle size (σ) (TEM) (nm) | Fitted to the data | Adjusted Eq. (11) | Particle size (nm) |
| 20 | 19 | 20 | 17 (2) | 7 | 6.9 | 16.9 |
| 20 | 19 | 95 | 19 (2) | 2.6 | 3.1 | 20.2 |
| 21 | 19 | 70 | 22 (2.5) | 4.8 | 4.4 | 21.3 |
| 24 | 19 | 40 | 20 (2) | 5.9 | 6.1 | 20.3 |
| 33 | 19 | 40 | 21(2) | 7 | 6.6 | 20.5 |
| 35 | 65 | 70 | 11 (1) | 1.7 | 1.7 | 10.9 |
| 42 | 4 | 20 | 24 (3) | 8.2 | 9.2 | 25.1 |
| 42 | 6 | 20 | 23 (3) | 9.5 | 9.0 | 22.6 |
| 42 | 12 | 20 | 19 (2) | 8.3 | 8.6 | 19.4 |
| 42 | 19 | 40 | 21 (2) | 7.4 | 7.0 | 20.7 |
| 43 | 19 | 70 | 23 (2.5) | 6.2 | 5.5 | 22.1 |
| 43 | 50 | 70 | 14 (1) | 2.9 | 3.2 | 14.6 |
| 48 | 6 | 20 | 23 (2) | 9.7 | 9.3 | 22.7 |
| 52 | 19 | 70 | 22 (2) | 5.8 | 6.0 | 22.3 |

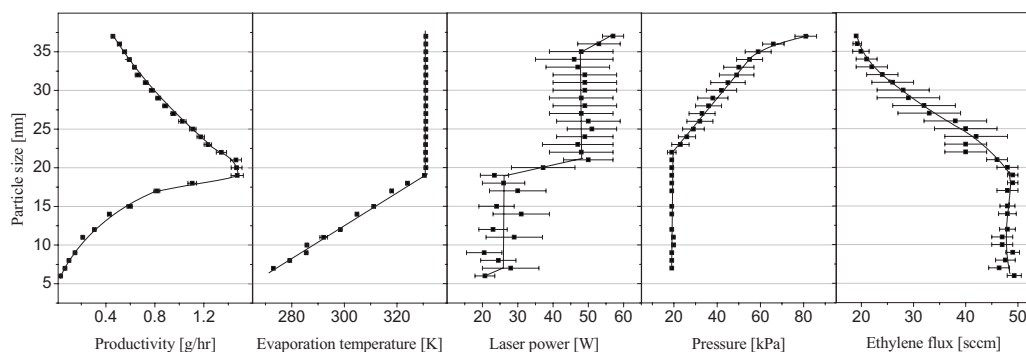


FIG. 6. Representation of the maximum productivity predicted by the model and the experimental conditions needed for the production of α -Fe nanocrystals of a given size.

$$t_c(\text{ms}) = 8.3 + 0.052W(\text{W}) - 0.075\Phi(\text{sccm}) - 0.051P(\text{kPa}) \quad (14)$$

($r=0.97$, 14 points, 6% error, 2–60 W, 19–65 sccm, 20–95 kPa).

The optimal agreement between the particle sizes obtained using the coagulation times calculated by Eq. (14) and the experimental ones shown in Table I indicates that the coagulation theory and our approximate determinations of the process temperature and coagulation time are accurate enough for the prediction of the iron particle size that can be obtained in the laser pyrolysis of iron pentacarbonyl.

2. Evaluation of the process parameters for an optimum production of iron nanoparticles by laser pyrolysis

By successive application of a coded computer program codified using MATHCAD code with Eqs. (1), (2), (11), (13), and (14), all the possible combinations of experimental conditions could be formed with the following discrete set of values: laser power (W): 19, 23, ..., 60; pressure (kPa): 19, 26.5, ..., 100; ethylene flux (sccm): 19, 22, ..., 65; and evaporation temperature (K): 273, 279, ..., 333. In order to make the results less sensitive to numerical artifacts, the computer program was provided with random variables that modified each of the variable inputs inside an interval of ± 2 units. Each run then operates with a slightly different set of input values and gives different results. After successive executions of the program (250 000 combinations of variables) for each particle size, the average of all the combinations of variables that resulted in a calculated production greater than 0.9 times the maximum is averaged. In Fig. 6, we show the combination of variables that make it possible to get the highest rates of production of nanoparticles as a function for each attainable particle size. The error bar represents the possible values of the control variable that guarantees the same productivity. Its magnitude represents how critical this parameter is for each case.

From the analysis of Fig. 6, it becomes obvious that the maximum productivity of nanoparticles is a function of the particle size, which was detected as having a critical value of 20 nm approximately. Therefore, the critical control variables that rule the system are different in regions below 20 nm and above 20 nm. A high yield of particles higher than 20

nm is obtained at high-evaporation temperatures (330 K) and high laser power (50 W) using the pressure and the ethylene flux as control variables, which means that in this region the main ruling factor is the residence time. On the contrary, below 20 nm the highest yields are obtained at high ethylene flux (50 sccm), low pressure (20 kPa), and low laser power (30 W) being the only ruling parameter of the precursor temperature or, in other words, the concentration of iron atoms in the reaction zone. The relatively low dependence of the results on the laser power is quite surprising.¹⁷ We suppose that this comes from the relatively low temperature of the process when compared with other laser pyrolysis synthesis and the assumption of instantaneous total decomposition of the precursor once the decomposition temperature is attained.

IV. CONCLUSIONS

In this work, the synthesis of iron ultrafine nanoparticles by laser pyrolysis is described using a coagulation model based on the aerosol theory. The calculations performed using this relatively simple model reproduce satisfactorily the average particle sizes measured by TEM for a variety of experimental conditions. The model is based on fundamental principles and only one adjustable parameter (the coagulation time) and is of general application for other laser pyrolysis processes. It could be employed for the evaluation of experimental parameters chosen in order to obtain a given average particle size.

ACKNOWLEDGMENTS

This work was supported by the Spanish Ministry of Science and Innovation through Project No. MAT2008-01489 and by the Institute for Health Carlos III through the Project of Biomedical Research (CIBER) Ref. No. CB 06/01/0026 (2007–2011).

¹J. Kim, Y. Piao, and T. Hyeon, *Chem. Soc. Rev.* **38**, 372 (2009).

²J. Cheon and J. H. Lee, *Acc. Chem. Res.* **41**, 1630 (2008).

³L. Frullano and T. J. Meade, *JBIC, J. Biol. Inorg. Chem.* **12**, 939 (2007).

⁴Q. A. Pankhurst, J. Connolly, S. K. Jones, and J. Dobson, *J. Phys. D: Appl. Phys.* **36**, R167 (2003).

⁵N. Rozanova and J. Z. Zhang, *J. Biomed. Nanotech.* **4**, 377 (2008).

⁶J. R. McCarthy and R. Weissleder, *Adv. Drug Delivery Rev.* **60**, 1241 (2008).

⁷P. Tartaj, M. P. Morales, T. González-Carreño, S. Veintemillas-Verdaguer, and C. J. Serna, *J. Magn. Mater.* **290–291**, 28 (2005).

- ⁸S. Laurent, D. Forge, M. Port, A. Roch, C. Robic, L. Vander Elst, and R. N. Muller, *Chem. Rev. (Washington, D.C.)* **108**, 2064 (2008).
- ⁹M. T. Swihart, *Curr. Opin. Colloid Interface Sci.* **8**, 127 (2003).
- ¹⁰R. W. Cannon, C. S. Danforth, J. H. Flint, S. J. Haggerty, and A. R. Marra, *J. Am. Ceram. Soc.* **65**, 324 (1982).
- ¹¹R. W. Cannon, C. S. Danforth, S. J. Haggerty, and A. R. Marra, *J. Am. Ceram. Soc.* **65**, 335 (1982).
- ¹²J. S. Haggerty and W. R. Cannon, in *Sinterable Powders from Laser-Driven Reactions in Laser Induced Chemical Processes*, edited by J. I. Steinfeld (Plenum, New York, 1981), p. 165.
- ¹³O. Bomati-Miguel, P. Tartaj, M. P. Morales, P. Bonville, U. Gollaschindler, X. Q. Zhao, and S. Veintemillas-Verdaguer, *Small* **2**, 1476 (2006).
- ¹⁴O. Bomati-Miguel, M. P. Morales, P. Tartaj, J. Ruiz-Cabello, P. Bonville, M. Santos, X. Zhao, and S. Veintemillas-Verdaguer, *Biomaterials* **26**, 5695 (2005).
- ¹⁵F. Erogbogbo, K. T. Yong, I. Roy, G. X. Xu, P. N. Prasad, and M. T. Swihart, *ACS Nano* **2**, 873 (2008).
- ¹⁶X. G. Li, Y. Q. He, S. S. Talukdar, and M. T. Swihart, *Langmuir* **19**, 8490 (2003).
- ¹⁷J. M. Lihmann and M. Cauchetier, *J. Eur. Ceram. Soc.* **13**, 41 (1994).
- ¹⁸P. E. Di Nunzio and S. Martelli, *Aerosol Sci. Technol.* **40**, 724 (2006).
- ¹⁹T. González-Carreño, M. P. Morales, M. Gracia, and C. J. Serna, *Mater. Lett.* **18**, 151 (1993).
- ²⁰X. X. Bi, B. Ganguly, G. P. Huffman, F. E. Huggins, M. Endo, and P. C. Eklund, *J. Mater. Res.* **8**, 1666 (1993).
- ²¹*Handbook of Chemistry and Physics*, 72nd ed., edited by R. David (CRC Press, Cleveland, 1991).
- ²²S. K. Friedlander, *Smoke, Dust and Haze: Fundamentals of Aerosol Behavior* (Wiley, New York, 1977).
- ²³E. Otto and H. Fissan, *Adv. Powder Technol.* **10**, 1 (1999).
- ²⁴D. A. McQuarrie, *Statistical Mechanics* (Harper & Row, New York, 1976), Chap. 16, pp. 357–372.
- ²⁵T. Majima, *Coord. Chem. Rev.* **132**, 141 (1994).
- ²⁶T. Majima, Y. Matsumoto, and M. Takami, *J. Photochem. Photobiol., A* **71**, 213 (1993).
- ²⁷L. De Dominicis, M. Di Fino, R. Fantoni, S. Martelli, O. Bomati Miguel, and S. Veintemillas Verdaguer, *Chem. Phys. Lett.* **348**, 209 (2001).